Published in final edited form as:
Circ Cardiovasc Imaging. 2018 August ; 11(8): . doi:10.1161/CIRCIMAGING.117.007303.

Tropoelastin: A novel marker for plaque progression and instability

Alkystis Phinikaridou, PhD[#1,2], **Sara Lacerda, PhD**[#1,2,†], **Begoña Lavin, PhD**[1,2], **Marcelo E. Andia, MD, PhD**[1,3], **Alberto Smith, PhD**[4], **Prakash Saha, PhD, FRCS**[4], and **René M. Botnar, PhD**[1,2,5,6]

[1]School of Biomedical Engineering Imaging Sciences, King's College London, London, UK

[2]BHF Centre of Excellence, Cardiovascular Division, King's College London, London, UK

[3]Radiology Department, School of Medicine, Pontificia Universidad Católica de Chile, Santiago, Chile

[4]Academic Department of Vascular Surgery, Cardiovascular Division, King's College London, London, UK

[5]Wellcome Trust and EPSRC Medical Engineering Center, King's College London, UK

[6]Pontificia Universidad Católica de Chile, Escuela de Ingeniería, Santiago, Chile

[#] These authors contributed equally to this work.

Abstract

Background—Elastolysis and ineffective elastogenesis favor the accumulation of tropoelastin, rather than cross-linked elastin, in atherosclerotic plaques. We developed gadolinium-labeled tropoelastin-specific magnetic resonance contrast agents (Gd-TESMAs) for tropoelastin imaging in animal models.

Methods and Results—Two peptides, VVGSPSAQDEASPLS and YPDHVQYTHY were selected to target tropoelastin. *In vitro* binding, relaxivity, and biodistribution experiments enabled characterization of the probes and selecting the best candidate for *in vivo* MRI. MRI was performed in atherosclerotic apolipoprotein E-deficient ($ApoE^{-/-}$) mice and New Zealand white rabbits with stable and rupture-prone plaques using Gd-TESMA. Additionally, human carotid endarterectomy specimens were imaged *ex vivo*. The VVGSPSAQDEASPLS-based probe discriminated between tropoelastin and cross-linked elastin (64±7% vs 1±2%, P=0.001), had high *in vitro* relaxivity in solution ($r_{1\text{-free}}$=11.7±0.6$mM^{-1}s^{-1}$, $r_{1\text{-bound to tropoelastin}}$ = 44±1$mM^{-1}s^{-1}$) and favorable pharmacokinetics. *In vivo* mice *v*ascular enhancement (4wks=0.13±0.007mm^2, 8wks=0.22±0.01mm^2, 12wks=0.33±0.01mm^2, P<0.001) and R_1 relaxation rate (4wks=0.90±0.01 s^{-1}, 8wks=1.40±0.03 s^{-1}, 12wks=1.87±0.04s^{-1}, P<0.001) increased with atherosclerosis

Correspondence address: Alkystis Phinikaridou, PhD, King's College London, School of Biomedical Engineering Imaging Sciences, 4th Floor, Lambeth Wing, St Thomas' Hospital, London SE1 7EH, United Kingdom, Tel: 077 1382 0192, Fax: 0207 188 5442, alkystis.1.phinikaridou@kcl.ac.uk.
[†]Current affiliation : Centre de Biophysique Moléculaire, CNRS, Orléans, France

Disclosures
None.

Europe PMC Funders Author Manuscripts

progression after Gd-TESMA injection. Conversely, statin-treated (0.13±0.01mm^2, R_1 =1.37±0.03s^{-1}) and control (0.10±0.005mm^2, R_1 =0.87±0.05s^{-1}) mice showed less enhancement. Rupture-prone rabbit plaques had higher R_1 relaxation rate compared with stale plaques (R_1=2.26±0.1s^{-1} *vs* R_1=1.43±0.02s^{-1}, *P*=0.001), after administration of Gd-TESMA that allowed detection of rupture-prone plaques with high sensitivity (84.4%) and specificity (92.3%). Increased vascular R_1 relaxation rate was observed in carotid endarterectomy plaques after soaking (R_{1pre}= 1.1±0.26 s^{-1} vs R_{1post}= 3.0±0.1s^{-1}, *P*=0.01). *Ex vivo* analyses confirmed the MRI findings and showed uptake of the contrast agent to be specific for tropoelastin.

Conclusions—MRI of tropoelastin provides a novel biomarker for atherosclerotic plaque progression and instability.

Introduction

Cardiovascular disease (CVD) accounts for nearly one-third of sudden and premature deaths worldwide1. Despite improvements in the management of patients, CVD related deaths are projected to affect 12 million people by 20302. Atherosclerosis is the underlying cause of the majority of cardiovascular events. Atherosclerotic plaque progression involves the dynamic turnover of the extracellular matrix (ECM) protein, elastin, through elastolysis3,4 (degradation) and elastogenesis (*de novo* synthesis)5–8. Elastolysis3,4 induced by inflammatory processes that upregulate the expression of elastases9 has been considered the major pathway for elastin remodeling. Conversely, dysfunctional elastogenesis and its contribution to plaque progression and instability, is less understood5–8.

Elastin is a highly abundant ECM protein found in the arterial wall that contributes to 50% of its dry weight10. Mature elastin is an insoluble and hydrophobic polymer, with a very low turnover rate. Mature elastin is formed by cross-linking of tropoelastin, a 60-72 kDa soluble monomer 11, by lysyl oxidase (LOX). Mature elastin contains several tropoelastin molecules. Tropoelastin has two alternating domains: (1) hydrophilic, cross-linked, domains rich in Lys and Ala and (2) hydrophobic domains (responsible for elasticity) rich in Val, Pro, and Gly, which often occur in repeats of VPGVG or VGGVG11. Endothelial cells, vascular smooth muscle cells (VSMCs) and adventitial fibroblasts produce tropoelastin during the late fetal and early neonatal periods of life, after which elastogenesis ceases11. Secreted tropoelastin is “chaperoned” to the extracellular space by the elastin-binding protein (EBP)12,13 where tropoelastin is stabilized and aligned along microfibrils, that contain glycoproteins (e.g. fibrillins) and microfibril-associated glycoproteins (e.g., MAGP-1) prior to enzymatic cross-linking14,15. Thus, normal arteries contain cross-linked elastin but negligible amounts of tropoelastin.

Dysfunctional ECM synthesis and degradation contribute to the initiation, progression and complication of arterial diseases including atherosclerosis6,16,17, abdominal aortic aneurysm (AAA)18, supravalvular aortic stenosis19, in-stent restenosis20,21 and Marfan’s syndrome22. In atherosclerosis, VSMCs23,24 and macrophages6,8 resume production of tropoelastin that often fails to cross-link into elastic fibers as a result of the reduced expression or absence of LOX25–30, or any of the components of the microfibrillar scaffold required for fiber assembly31–33. Simultaneously, elastin degradation by elastases9

Europe PMC Funders Author Manuscripts

generates elastin-derived peptides, including the VGVAPG, that are chemotactic for inflammatory cells34, participate in lipoprotein retention, and upregulate matrix metalloproteinases10, all of which are involved in the progression and instability of a plaque.

Over the past 10 years there have been significant developments in imaging of molecular components of the vessel wall *in vivo*. Imaging of vascular elastin has been achieved using the elastin-specific MRI contrast agent (ESMA)35 in preclinical models of atherosclerosis36–38, AAA39, coronary artery injury40 and myocardial remodeling after infarction41,42. Collagen-binding paramagnetic nanoparticles have also successfully been used to image collagen remodeling in murine atherosclerosis43; while *in vivo* optical analysis has been used to quantify changes in collagen and elastin after wall injury44.

As elastogenesis and elastolysis favor the accumulation of tropoelastin, rather than fully processed cross-linked elastin, we hypothesized that tropoelastin may serve as a new imaging biomarker to detect atherosclerosis progression and lesion instability. Herein, we have developed, characterized and validated novel tropoelastin-specific MR contrast agents to image tropoelastin turnover in models of atherosclerosis and plaque instability and shown potential to bind to symptomatic plaques taken from patients undergoing carotid endarterectomy.

Methods

The data, analytic methods, and study materials will not be made available to other researchers for purposes of reproducing the results or replicating the procedure.

Elastin and tropoelastin-binding probes

The tropoelastin peptides were selected as described in the online Supplementary Methods. The probes, (DOTA)-VVGSPSAQDEASPLS and K(DOTA)YPDHVQYTHY, their corresponding scrambled versions DOTA-GAESAPLVSSVQSPD (scrambled-V) and K(DOTA)-HQVYTYPHDY (scrambled-Y), as well as the rhodamine-labeled VVGSPSAQDEASPLS peptide derivative were custom synthesized by Peptide Synthetics Ltd. (Hampshire, UK). The DOTA-peptides were complexed in house with lanthanide ions: europium (Eu^{3+}), lanthanum (La^{3+}) or gadolinium (Gd^{3+}) for *in vitro* binding assays, relaxivity and MRI experiments; or $^{64}Cu^{2+}$ for biodistribution studies. The complexed (DOTA)-VVGSPSAQDEASPLS and K(DOTA)YPDHVQYTHY probes were denominated as tropoelastin-binding MR contrast-agents (TESMAs). The diethylenetriaminepentaacetic acid (DTPA)-based elastin-specific contrast agent was provided by Lantheus Medical Imaging (North Billerica, USA)35, either complexed to gadolinium, (Gd-ESMA; 856 Da) for relaxivity and MRI experiments or in its free form (ESMA), complexed in house with Eu^{3+} for *in vitro* binding assays. Eu^{3+} labeled DTPA solutions (Eu-DTPA) complexed in house were used as controls.

Synthesis of the lanthanide(III) complexes, *in vitro* binding and relaxivity studies were performed as described in the online Supplementary Methods.

Europe PMC Funders Author Manuscripts

Murine model of atherosclerosis progression

Male apolipoprotein E knockout ($ApoE^{-/-}$) mice and wild-type (WT) C57BL/6J were purchased from Charles Rivers Laboratories (Edinburgh, UK). 8 week-old $ApoE^{-/-}$ mice were switched to a high-fat diet (HFD) containing 21% fat from lard, and 0.15% (wt/wt) cholesterol (Special Diets Services, Witham, UK). $ApoE^{-/-}$ mice were imaged at 4, 8, and 12 weeks after HFD-feeding (n=10 per group). In the treatment group, $ApoE^{-/-}$ mice (n=10) received pravastatin (40mg/kg/day) (Kemprotec Ltd, Middlesborough, UK) administered in the drinking water simultaneously with the HFD for 12 weeks. 8 week-old WT mice (n=10) were fed a normal chow diet for 12 weeks and scanned at 20-weeks.

Rabbit model of plaque instability

Six 3 month-old male New Zealand White rabbits (Harlan, Wyton, England; mean weight, 2.5 kg) were fed a 1% cholesterol diet (Special Diet Services, Witham, England) for 2 weeks before and 6 weeks after balloon injury of the abdominal aorta. This was followed by 4 weeks of normal chow diet as previously described37,45,46. Diseased rabbits received intraperitoneal administration of Russell's viper venom (0.15 mg/kg; Enzyme Research Laboratories, Swansea, UK), a procoagulant factor, followed 30 minutes later by intravenous administration of histamine dihydrochloride (0.02 mg/kg; Sigma-Aldrich, Dorset, England), a vasoconstrictor in rabbits, to induce plaque disruption and thrombosis. This procedure was repeated twice within 4 hours. All procedures were approved by the United Kingdom Home Office and were in accordance with institutional guidelines.

Biodistribution of ^{64}Cu-labeled tropoelastin probes

Biodistribution experiments are described in the Online Supplementary Methods.

In vivo molecular imaging of tropoelastin at 3T

All imaging experiments were performed using a 3T Philips Achieva MR scanner (Philips Healthcare, Best, The Netherlands) equipped with a clinical gradient system (30mT m^{-1}, 200mT/m/ms).

Mice—Mice (n=10 per group) were imaged using a single–loop surface coil (diameter=23mm). The animals were placed in prone position and the brachiocephalic artery was imaged 30-40min post injection of the tropoelastin-binding contrast agent Gd-TESMA [(Gd-DOTA)-VVGS] (0.2mmol/kg). A subgroup of animals (n=5 per group) was also scanned 1h (optimal time point) after injection of Gd-ESMA (0.2mmol/kg) on the previous day for comparison (Online Supplementary Data Figure 1A). Additionally, 12 weeks HFD-fed animals (n=3) were imaged 30-40min after injection of the scrambled-VVGS probe (0.2mmol/kg), and another 2 mice were imaged with a 1:1 (Gd-TESMA + La-TESMA) cocktail for *in vivo* competition experiments. A detailed MRI acquisition protocol is described in the online Supplementary Methods.

Rabbits—The abdominal aorta of diseased rabbits was scanned using a 32-channel cardiac coil. Rabbits received general anaesthesia and were imaged in a supine position twice before (pre) and one time after (post) pharmacological triggering (Online Supplementary Data 1B).

The pre-trigger MR imaging included two separate scanning sessions; one before and after administration of Gd-ESMA and one before and after administration of Gd-TESMA. The second MRI session was performed two days after the first to allow vessel wall clearance of Gd-ESMA. During these sessions, native zoom T1-weighted black-blood (BB) and delayed-enhanced (DE) images and T1 maps were acquired 2h after administration of Gd-ESMA (0.2 mmol/kg) and 40min after administration of Gd-TESMA (0.2 mmol/kg). After the second scan, the rabbits were triggered twice for plaque rupture and the final post-triggering MR imaging session was performed 8h later. The post-trigger MRI included acquisition of native zoom T1-weighted BB images to visualize thrombus. A detailed MRI acquisition protocol is described in the online Supplementary Methods.

Ex vivo T1 mapping experiments using symptomatic plaques taken from patients undergoing carotid endarterectomy at 3T

Fresh symptomatic carotid endarterectomy specimens were imaged before and after soaking the in Gd-TESMA (Online Supplementary Data Figure 1C). A detailed tissue handling and MRI acquisition protocol is described in the online Supplementary Methods. Collection and use of human samples was approved by an institutional review committee and subjects gave informed consent.

MRI image analysis

In mice, vessel wall area was calculated by manually segmenting the visually enhanced region of the vessel wall as seen on the DE-MRI images using OsiriX (OsiriX Foundation, Geneva, Switzerland). To ensure that the segmented area encompassed the vessel wall the DE-MRI images were co-registered and fused with the magnetic resonance angiography images. T_1 values were computed on a pixel-by-pixel basis using a 3 parameter fit implemented in Matlab36. In rabbits, pre-trigger native T1w-BB images and contrast enhanced IR and T1 maps were used to assess the vascular remodelling. Post-trigger native T1w-BB images were only used to identify the presence or absence of thrombus as an endpoint for the classification of plaques as rupture-prone and stable, respectively. The T1 maps were automatically generated after the data acquisition using a 3-parameter fit model. The T1 maps were imported into Osirix and the vessel wall was manually segmented to calculate the R_1. When segmenting the T1 maps the anatomical T1w-BB images were used to aid the identification of the vessel wall contours. The analysis was performed on anonymized datasets in all experiments. T1 maps of *ex vivo* carotid endarterectomy specimens were analyzed as described above for the rabbit images.

Histology

Mice—The aortic root, aortic arch, brachiocephalic and carotid arteries were removed *en bloc*, pinned down to maintain tissue morphology and fixed in 10% formaldehyde for 48h (n=4 per group). Tissues were embedded in paraffin and sectioned transversely (5-μm thick). Verhoeff-Van Gieson elastin staining (HT25A-1KT, Sigma, Dorset, UK) and Trichrome Stain (Masson) Kit (HT15-1KT, Sigma, Dorset, UK) were used to investigate vessel wall morphology and elastin and collagen fibres, respectively. Immunohistochemistry for tropoelastin was performed using an anti-mouse rabbit polyclonal antibody (1:100, Abcam,

ab21600, Cambridge, MA, USA). Vessel wall area was calculated using the Verhoeff-Van Gieson images as [adventitia area−the luminal area (mm^2)] using ImageJ (NIH). The immunopositive areas were segmented and expressed as normalized tropoelastin area (%tropoelastin= tropoelastin immunopositive area/vessel wall area) × 100. Fluorescent microscopy was performed using a custom synthesized rhodamine-labeled VVGS peptide derivative (rhod-VVGS). Sections were incubated with a 200nM solution for 24h at 4°C followed by nuclear counterstain using Hoechst (ThermoFischer 33342, 1:3000, for 15 min at room temperature). Slides were shielded from light at all times and mounted with a Mowiol containing 2.5% 1,4-diazobicyclo-[2.2.2]-octane (DABCO, Sigma, D2522) medium.

Rabbits—Transverse cryosections (10μm thick) were collected throughout the length of each segment at 500μm intervals and stained with Verhoeff-Van Gieson to visualize the elastin fibres and calculate the total elastin content. Immunohistochemistry for tropoelastin was performed using an anti-mouse rabbit monoclonal antibody (1:100, NB100-2076, Novus Biologicals, Abingdon, UK). Computer-assisted colour image analysis (ImageJ) was used to quantify the percentage total elastin and tropoelastin content, using the Verhoeff-Van Gieson elastin and tropoelastin immunohistochemistry stainings, respectively. For registration of the *in vivo* MR images and histologic sections, the distance of the proximal end of each segment from the renal branches and iliac bifurcation, the gross morphology, and internal plaque and/or thrombus landmarks visible on both the MR and histologic images were used as references.

Human carotid endarterectomy (CEA) specimens—After the imaging experiments, the plaques from endarterectomy were fixed in formalin, decalcified, embedded in paraffin, and sectioned transversely at 5μm. Sections were stained for collagen using Masson's trichrome, elastin with Verhoeff-Van Gieson and tropoelastin by immunohistochemistry (1:100, Abcam, ab21600, Cambridge, MA, USA).

Western Blot experiments for quantification of vessel wall tropoelastin concentration are described in the online Supplementary Methods.

Inductively coupled plasma mass spectrometry (ICP–MS) was used to quantify vessel wall gadolinium concentrations as described in the online Supplementary Methods.

Statistical analyses

The detailed statistical methods are described in the online Supplemental Methods. *P*-values <0.05 were considered statistically significant.

Results

Chemical structures and *in vitro* binding assays

The chemical structures and molecular weight of the gadolinium-labelled tropoelastin-binding probes are shown in Figures 1A-B. *In vitro* binding experiments showed that both K(Eu-DOTA)-YPDH and (Eu-DOTA)-VVGS probes have high selectivity towards tropoelastin compared with other proteins including collagen I, fibronectin, and human

serum albumin (HSA) (Figure 1C). Importantly, the (Eu-DOTA)-VVGS probe showed superior discrimination between tropoelastin and mature elastin (64±7% vs 1±2%, *P*=0.001) compared with K(Eu-DOTA)-YPDH (84± 4% vs 53±5%, *P*=0.009). Conversely, Eu-ESMA showed equal binding to tropoelastin and mature elastin (40±1% vs 41±2%, *P*=NS). Additionally, both (Eu-DOTA)-VVGS and K(Eu-DOTA)-YPDH did not show binding to HSA, whereas Eu-ESMA has been reported to bind 15% to HSA [value included in Figure 1C40]. Finally, Eu-DTPA and complexes of the scrambled VVGS and YPDH probes showed no binding to all proteins studied. The saturation binding plots (Figure 1D-E) showed that both probes bind to tropoelastin whereas no binding to HSA was observed. Finally, no binding of the scrambled probes to tropoelastin was observed. The K_D values showed high affinity of the probes towards tropoelastin (Figure 1F). Further competition studies showed the specificity of the two probes (Online Data Supplement Figure 2).

Relaxivity studies using Gd-labeled tropoelastin and elastin-binding contrast agents

^{1}H nuclear magnetic relaxation dispersion (NMRD) profiles obtained in PBS were characteristic of small-molecular weight complexes (Figure 2A-C). As expected, the relaxivity values of the new probes were higher (r_1 =8.9±0.4 and 11.7±0.6$mM^{-1}s^{-1}$ for K(Gd-DOTA)-YPDH and (Gd-DOTA)-VVGS, respectively, at 20MHz and 37°C) compared with non-peptide based contrast agents (e.g., Gd-DTPA=4.02$mM^{-1}s^{-1}$ at 20MHz, 37°C)47 (Figure 2D) due to the increased molecular weight (reducing the rotational correlation time), which also contributes to second- and outer-sphere proton relaxation effects47. The relaxivity of Gd-ESMA was measured to be 4.9±0.3$mM^{-1}s^{-1}$ (20MHz, 37°C).

In the presence of tropoelastin (TE), the relaxivity of the bound fraction was calculated taking into account the K_D and a stoichiometry of 1:2 tropoelastin:probe as determined by the fluorescence studies (Figure 1F) and was plotted as a function of the magnetic field strength (Figure 2A-C). These NMRD profiles correspond to slow tumbling systems with a typical high field peak around 20-40MHz showing overall higher relaxivity for the tropoelastin-bound fraction: 36±1, 44±1 and 25±1$mM^{-1}s^{-1}$ for TE-[K(Gd-DOTA)-YPDH)], TE-[(Gd-DOTA)-VVGS)], and TE-[(Gd-ESMA)], respectively.

To investigate the metabolic stability of all Gd-probes we measured the R_1 relaxation rates of 1mM solution of the probes incubated with murine and human blood and plasma every 30min, up to 4h at 3T. These data showed that the probes were stable in solution for up to 4h as the changes in the R_1 relaxation rate were not statistically significant (data not shown).

Biodistribution of ^{64}Cu-labeled tropoelastin probes

Biodistribution studies showed favorable pharmacokinetics with high renal clearance for both probes and some liver uptake for the K(^{64}Cu-DOTA)-YPDH (Online Data Supplement Figure 3).

In vivo comparison of vessel wall enhancement by MRI using the elastin (ESMA) and tropoelastin binding (TESMA) contrast agent

Considering that (Gd-DOTA)-VVGS was superior in differentiating tropoelastin from cross-linked elastin and had less liver uptake compared to the K(DOTA)-YPDH imaging probe,

the (Gd-DOTA)-VVGS, denominated as Gd-TESMA, was selected as the best candidate for *in vivo* molecular imaging of tropoelastin by MRI. For initial *in vivo* MRI experiments, control and atherosclerotic ApoE$^{-/-}$ mice were scanned, after the administration of Gd-ESMA, and 24h later, after the administration of Gd-TESMA (Figure 3). Pilot studies showed clearance of Gd-ESMA from both the blood and vessel wall after 24h **(data not shown)**. Fused maximum intensity projection (MIP) MRA and delayed-enhanced (DE) images after injection of Gd-TESMA showed focal uptake in the brachiocephalic artery (BCA) of an atherosclerotic mouse (Figure 3A). DE-MRI images of the BCA acquired from a control animal after injection of Gd-ESMA showed vessel wall enhancement (Figure 3B-C), as Gd-ESMA binds to endogenously found cross-linked elastin, present in non-diseased arteries. Conversely, there was no enhancement of the control vessel wall after injection of Gd-TESMA due to the lack of tropoelastin in the absence of disease (Figure 3D-E). However, two different atherosclerotic mice, showed enhancement of the vessel wall after administration of both Gd-ESMA and Gd-TESMA (Figure 3F-M). DE-MRI showed a larger area of enhancement after administration of Gd-ESMA compared with Gd-TESMA as the diseased vessel wall contains a mixture of cross-linked elastin and tropoelastin and Gd-ESMA binds to both fractions whereas Gd-TESMA only binds to tropoelastin (also see Figure 1C & online Data Supplement Figure 4A-B).

In vivo molecular MRI of tropoelastin shows accumulation of tropoelastin during atherosclerosis progression in mice

DE-MRI (Figure 4A_1-D_1 & 4A_2-D_2) and R_1 maps (Figure 4A_3-D_3) acquired after administration of Gd-TESMA showed progressive enhancement and increased vessel wall R_1 relaxation rate of the BCA in ApoE$^{-/-}$ mice exposed to a HFD compared with wild-type mice. Statin-treated ApoE$^{-/-}$ mice showed significantly less enhancement and lower relaxation rate compared with untreated ApoE$^{-/-}$ mice (Figure 4$E_{1\text{-}3}$) The uptake of Gd-TESMA by DE-MRI and R_1 mapping paralleled the growth of atherosclerotic lesions (Figure 4A_4-E_4) as seen by Van Gieson elastin staining and the deposition of tropoelastin fibers as seen by immunostaining (Figure 4A_5-E_5, Figure 4A_6-E_6 and Figure 4A_7-E_7). The higher magnification images (Figure 4A_6-E_6) of tropoelastin immunopositive areas (black signal) show that the antibody does not bind to endogenously and cross-linked elastin found in the media of control arteries and even in tissues from animals fed with a HFD for 4 weeks. However, as the disease progresses and new tropoelastin fibers are deposited within the growing intima, and also as media elastin becomes fragmented by elastases, the immunopositive areas increase in both of these layers of the vessel wall. ApoE$^{-/-}$ mice fed a HFD for 12 weeks showed less vessel wall enhancement after administration of the scrambled peptide probe (DOTA-GAESAPLVSSVQSPD) compared with those injected with the non-scrambled probe (Figure 4F_1-F_3). *In vivo* competition experiments showed displacement of the (Gd-DOTA)-VVGS probe by the (La-DOTA)-VVGS probe in the brachiocephalic artery of atherosclerotic mice (on line Data Supplement Figure 5). *Ex vivo* fluorescent microscopy experiments showed fluorescent signal originating from the rhodamine-labeled VVGS peptide derivative within tropoelastin-rich areas of diseased vessels as identified by corresponding immunohistochemistry. Conversely, fluorescent signal originating from the probe was found to be nearly non-existent in the regions containing

Europe PMC Funders Author Manuscripts

mature/crosslink elastin-rich and collagen in diseased vessels (on line Data Supplement Figure 6).

Quantitative MRI, histology and western blot measurements of murine vessel wall tropoelastin

Quantification of the MR data showed that the DE-MRI area (Figure 5A, control=0.10±0.005, 4wks=0.13±0.01, 8wks=0.22±0.01, 12wks=0.33±0.01mm^2, P<0.001) and the vessel wall R_1 (Figure 5B, control=0.87±0.05, 4wks=0.90±0.01, 8wks=1.40±0.03, 12wks=1.87±0.04s^{-1}, P<0.001) significantly increased with disease progression and decreased with statin-treatment (DE-MRI treated=0.13±0.01mm^2, R_1 treated=1.37±0.03s^{-1}). Less uptake was found in 12wk-old HFD-fed ApoE$^{-/-}$ mice injected with a scrambled peptide of VVGS (0.13±0.01mm^2 vs 0.33±0.01, P=0.001) and lower R_1 (0.91±0.06 vs 1.87±0.04, P=0.01) compared with animals injected with the non-scrambled Gd-TESMA peptide. Segmentation of the tropoelastin immunopositive areas showed a significant accumulation of tropoelastin fibers during atherosclerosis progression and reduction of tropoelastin in the statin-treated ApoE$^{-/-}$ mice (% tropoelastin, control mice=3.8±0.50, 4wks HFD =3.74±0.60, 8wks HFD =12.10±0.52, 12wks HFD =18.54±0.30, statin-treated at 12wks with HFD =11.41±0.35, P=0.002) (Figure 5C). Quantification of the vessel wall gadolinium concentration by ICP-MS showed similar trends (control=176±50, 4wks=165±38, 8wks=244±52, 12wks=303±38, statin-treated at 12wks=207±23 nmol/gr tissue, P=0.007) (Figure 5D). There was a significant correlation between the vessel wall R_1 and gadolinium concentration [r=0.97, P=0.004, 95% CI (0.69-0.99)]. A linear regression analysis of average R_1 and average [Gd] per time point of disease progression revealed an *in vivo* bound relaxivity of r_1=7.15 mM^{-1}s^{-1} (Figure 5E).

We found a significant correlation between the DE-MRI plaque area and vessel wall R_1 measured after administration of Gd-TESMA (r=0.58, P<0.001, 95% CI=0.46-0.69) (Figure 5F). There were also strong positive correlations between plaque % tropoelastin (measure immunohistochemically) and both the *in vivo* DE-MRI area (r=0.76, P<0.001, 95% CI=0.47-0.89) (Figure 5G) and vessel wall R_1 (r=0.93, P<0.001, 95% CI=0.76-0.96) (Figure 5H) suggesting that the increased MRI signal observed in this model reflects the histological accumulation of tropoelastin fibers within the growing lesion.

In addition to the quantification of tropoelastin by immunohistochemistry (Figure 5C), the modulation of the protein levels during atherosclerosis progression and in response to treatment were also measured by western blotting. Dilutions of recombinant tropoelastin were used to generate a standard curve for the quantification of the tropoelastin concentration from tissue lysates (Figure 5I). Western blotting of purified cross-linked elastin and soluble tropoelastin showed that the cross-linked polymer gives a high molecular weight band (>250kDa) whereas the tropoelastin monomer has a molecular weight of 70kDa (Figure 5J). Western blotting of tropoelastin extracted from the vessel wall showed negligible amounts in control arteries and increased deposition during atherosclerosis progression in ApoE$^{-/-}$ mice. Tropoelastin content was decreased in statin-treated ApoE$^{-/-}$ mice (Figure 5J). Quantification of tropoelastin concentration in control and diseased

arteries is shown in Figure 5K (control=0.62±0.04, 4wks=0.86±0.05, 8wks=1.52±0.06, 12wks=1.99±0.15, statin-treated at 12wks=1.17±0.09 mg/gr tissue, $P<0.001$).

In vivo molecular MRI of tropoelastin allows detection of rupture-prone rabbit plaque

To test the ability of molecular MRI of tropoelastin in discriminating between stable and rupture-prone plaques we used a rabbit model of atherosclerosis and controlled plaque rupture. Atherosclerosis was observed at 12-weeks in all 6 injured and cholesterol-fed rabbits, and thrombosis occurred in 5 (83%) animals at rates similar to those previously reported37,45,46,48. Figure 6 shows corresponding native T1wBB, delayed-enhanced images and T_1 maps after administration of Gd-ESMA and Gd-TESMA acquired at 12 weeks and before triggering for plaque rupture and native T1wBB images acquired after triggering for plaque rupture. Representative pre-trigger T1wBB images of a stable (Figure 6A-E) and rupture-prone plaques (Figure 6G-K) show the anatomy of the vessel wall and the location of the plaque. The delayed-enhanced images show an enhancement of the vessel wall and shortening of the T1 relaxation time both after the administration of Gd-ESMA and also after the administration of Gd-TESMA. The corresponding T1wBB images acquired after triggering show the lack of thrombus at the level of the stable plaque and the presence of thrombus at the location of the rupture-prone lesion (Figure 6F and 6L). Although both Gd-ESMA and Gd-TESMA lead to vessel wall enhancement, quantitative assessment of the R_1 relaxation rate showed that the uptake of contrast agent was significantly different between stable and rupture-prone lesions only after administration of Gd-TESMA (Figure 6M). Rupture-prone plaques uptake significantly more Gd-TESMA compared with stable plaques (R_1=2.26±0.1 *vs* R_1=1.43±0.02, P=0.001) whereas the uptake of Gd-ESMA was similar between stable and rupture-prone plaques (R_1=2.14±0.05 *vs* R_1=2.44±0.07, P=NS). The sensitivity, specificity, positive predictive value and negative predictive value of the quantitative assessment of vascular elastin and tropoelastin (R_1) after administration of Gd-ESMA and Gd-TESMA, respectively in detecting the rupture-prone plaque are tabulated in Figure 6N. These measurements suggest that quantitative assessment of vessel wall contrast uptake using T_1 mapping after administration of Gd-TESMA allows better *in vivo* detection of rupture-prone plaques.

Histological analyses show accumulation of tropoelastin in rabbit rupture-prone compared with stable plaque

Histological analyses of rabbit sections using Van Gieson elastin showed multiple elastin lamellae consisting of mature, cross-linked elastin in control arteries (Figure 7A; **black stain**) but no corresponding immunopositive tropoelastin fibers suggesting the antibody is specific for monomeric tropoelastin (Figure 7B and 7C).

In both stable and ruptured plaques there was deposition of elastin in the intima (Figure 7D, 7G) and in ruptured plaques there was also additional disintegration and fragmentation of the media elastin as seen by Van Gieson elastin. Immunohistochemistry for tropoelastin (brown stain) showed deposition of tropoelastin in the intima of stable plaque (Figure 7E-F) and a more extensive network of tropoelastin in the intima of ruptured plaque (7H-I). In addition, there were immunopositive tropoelastin areas in the media of ruptured plaques that could be due to either deposition of new tropoelastin fibers or exposure of the tropoelastin

epitope when mature elastin fibers become fragmented by elastases. Quantification of total elastin and tropoelastin (Figure 7J-7K) showed that measuring the tropoelastin accumulation in the vessel wall allowed a better discrimination between stable and ruptured plaques (16.6±3.14 *vs* 42.2±4.0, P=0.001) compared with measuring the net increase of elastin (28.8±3.0 *vs* 44.35±4.83 %, P=0.03) that includes both the cross-linked and non cross-linked elastin fibers. Only negligible amounts of tropoelastin (7.3±1.45%) were found in control vessel wall segments compared with elastin (26.3±0.9%).

Ex vivo molecular MRI of tropoelastin in human carotid endarterectomy samples

To test the translational value of the tropoelastin contrast agent we performed *ex vivo* T_1 mapping experiments after soaking the tissues in Gd-TESMA. The MRI results showed retention of Gd-TESMA and significant increase in the R_1 relaxation rate of carotid plaques ($R_{1\ pre}$= 1.1±0.26s^{-1} vs $R_{1\ post}$= 3.0±0.1s^{-1}, P=0.01) (Figure 8A-E) and the histological analyses showed upregulation of tropoelastin in the lesion (Figure 8F-H).

Discussion

Elastolysis and ineffective elastogenesis favor the accumulation of tropoelastin, rather than mature cross-linked elastin fibers, in atherosclerosis and may trigger plaque progression and instability (6). We have identified tropoelastin-binding peptides and developed a novel gadolinium-based tropoelastin-binding contrast agent that can be used for MR imaging of tropoelastin turnover in atherosclerosis. We demonstrate that the newly developed Gd-TESMA probe (Gd-DOTA)-VVGS: (i) has high selectivity for tropoelastin, (ii) discriminates between tropoelastin and cross-linked elastin, (iii) has high *in vitro* relaxivity (r_1) that increases upon binding to tropoelastin in solution, and (iv) has favorable pharmacokinetics with blood clearance within 1h via renal excretion. Using (Gd-DOTA)-VVGS, we demonstrate, for the first time, the feasibility of *in vivo* imaging of tropoelastin turnover in a murine model of atherosclerotic plaque progression and response to treatment and in a rabbit model of plaque instability. In addition, we show the potential for this novel contrast agent to bind to symptomatic plaques taken from patients undergoing carotid endarterectomy. Molecular imaging of tropoelastin in mice showed increased vessel wall enhancement and R_1 relaxation rates during plaque progression compared with statin-treated and control animals. Histology and western blotting confirmed the accumulation of tropoelastin within the growing lesion and ICP-MS confirmed the accumulation of gadolinium in the vessel wall. Molecular imaging of tropoelastin in rabbits showed significantly higher R_1 relaxation rates in rupture-prone compared with stable lesions showing potential for the detection of high-risk plaques with high sensitivity and specificity. Finally, molecular imaging of human carotid endarterectomy specimens showed detection of intra-plaque tropoelastin after soaking the tissues in Gd-TESMA suggesting that this contrast agent has potential in man. Non-invasive quantification of dysfunctional tropoelastin turnover, that fails to cross-link into mature elastin fibres, using a newly developed tropoelastin-binding MR contrast agent may therefore have diagnostic value in detecting not only plaque progression and response to treatment but also detection of unstable atherosclerotic lesions prior to plaque rupture.

The main targeted Gd-based low molecular weight contrast agents that have been developed bind to proteins including fibrin (EP-1873 and EP-2104R)49, collagen (EP-3533 and EP-3600)50,51, and elastin (BMS 753951 and LMI 1174)35,41,47 that are highly abundant and thus amenable for MR imaging. Most of these agents were initially developed as DTPA chelates and then modified to DOTA chelates, to increase their thermodynamic and kinetic stability49, and all are clear from blood within 1-2h after injection. Compared to these agents, our new tropoelastin agent with a single Gd-DOTA conjugated to the N-terminal of the 15 amino-acid peptide (2kDa), showed comparable affinity ($K_D \approx \mu M$), relaxivities and pharmacokinetics to these agents35,36,40,49–51.

Previous studies have shown that the VVGS12,13,52 probe is expected to bind to all sequences that follow the GXXPG and XGXPG motif (where X is a hydrophobic amino acid) that repeats multiple times in the tropoelastin molecule. In murine tropoelastin, these commonly repeated sequences represent 21% of the entire molecule53 that may explain our observation of higher vessel wall ICP-MS gadolinium measurements compared with the tropoelastin concentration as measured by western blotting. The *in vivo* vessel wall bound relativity of (Gd-DOTA)-VVGS was 7.15 $mM^{-1}s^{-1}$ and the image acquisition window lasted up to 1.5h post-injection. As some of the binding sites of tropoelastin might be masked and the amount of water is lower within the atherosclerotic lesion this could explain why the *in vivo* bound relaxivity was lower compared with the relaxivity in solution. Future improvements of the chemical properties of the agent, e.g., by chelating more Gd^{3+} per peptide, or conjugating the peptide to a different chelate unit that enables two water molecules in the inner coordination sphere of Gd^{3+} could increase the relaxivity of the free, but more importantly of the bound fraction of the agent, and also prolong the imaging acquisition window to allow better detection of vascular tropoelastin and imaging of larger vascular segments.

Our finding that tropoelastin accumulates within the growing lesion and reduces with statin-treatment (using immunohistochemistry and western blotting) in $ApoE^{-/-}$ mice is in agreement with a previous study36. Using western blotting we found that tropoelastin accumulation is up to 4-fold increased in the murine plaque, compared with control tissue, and reaches a concentration of about 2mg/gr of tissue. Although statins directly reduce plaque burden through a lipid-lower mechanism, they were also shown to abolish the down-regulation of LOX produced by tumour necrosis factor-α (TNFα) and LDL particles through a RhoA/Rho kinase-dependent mechanism27. Normalization of LOX could promote cross-linking of the newly synthesized tropoelastin leading to an overall reduction of tropoelastin, as seen in our study.

When compared with the Gd-ESMA, the new tropoelastin-agent resulted in a smaller area of contrast uptake at the same time points by MRI in atherosclerotic $ApoE^{-/-}$ mice. A previous study also reported a higher uptake of (^{153}Gd-DTPA)-ESMA compared with (^{64}Cu – DOTA)-VVGS (13.2 vs. 7.2 %ID/g)41. As shown in this and other studies36–38,40 Gd-ESMA binds equally to cross-linked elastin and tropoelastin. For this reason, enhancement of endogenous cross-linked elastin in non-diseased arteries was also observed in both mice and rabbits. To this end, Gd-ESMA allows measurement of total elastin content and the percentage increase that occurs from the control to the diseased condition by MRI.

Europe PMC Funders Author Manuscripts

In our current study, we found that quantitative assessment of vessel wall contrast uptake using T_1 mapping after administration of Gd-TESMA improved the detection of rupture-prone plaques compared with Gd-ESMA. Rabbit rupture-prone plaques uptake significantly more Gd-TESMA (higher vessel wall R_1) compared with stable plaques whereas the uptake of Gd-ESMA was similar between the two groups (similar R_1 values). The elimination of signal from endogenously present cross-linked elastin, and detection of only immature tropoelastin, using the Gd-TESMA, agent allowed a stronger discrimination between rupture-prone and stable rabbit plaques and high prediction of unstable lesions compared with Gd-ESMA. In our previous study using the same rabbit model37, we showed that administration of Gd-ESMA allowed measurement of plaque burden, that was significantly increased in diseased vessel walls (higher R_1) compared with control vessels and also improved the assessment of positive vascular remodeling that predicted rupture-prone plaques. Finally, to determine whether tropoelastin could be imaged in human tissue we carried out *ex vivo* T_1 mapping experiments in carotid plaque samples obtained from endarterectomy and soaked in Gd-TESMA. The MRI results showed retention of the agent in carotid plaques and the histological analyses revealed increased levels of tropoelastin in these plaques. Our findings are in agreement with studies demonstrating that synthetic VSCMs24,54 and macrophages6,8 secrete tropoelastin in rabbit atherosclerotic plaque and human carotid atheroma.

In conclusion, this study shows that the accumulation of tropoelastin is associated with plaque progression and instability in atherosclerotic models. In addition, the novel contrast agent is able to demonstrate the presence in tropoelastin in symptomatic plaques taken from patients supporting a potential role for this novel contrast agent in man.

Study Limitations

Our findings on the value of tropoelastin as a marker of plaque burden and instability relies on the use of animal models of atherosclerosis that reflect, only partly, the complex composition of human atherosclerotic plaques and their evolution towards rupture. Although a small intermediate step of using *ex vivo* human endarterectomy specimens was used to show the translational potential of our work, future studies including larger numbers of human samples will be needed. In addition, the ability of molecular imaging of tropoelastin to detect rupture-prone plaques was based on a relatively small a number of rabbits, larger animal studies will be need to confirm these findings.

A potential limitation of our study is that an independent black-blood (e.g., double inversion recovery) sequence for the entire vessel wall anatomy was not acquired for the murine experiments. Instead, we implemented a flow-independent delayed-enhancement MR imaging protocol that was clinically established for myocardial infarction and coronary vessel wall imaging in humans instead of a flow–dependent black-blood (BB) MR imaging. Another limitation our study was the lack of an automated/semi-automated software for region-of-interest (ROI) analysis, which was performed manually for all experiments. Future implementation of threshold-based segmentation algorithms may improve vessel wall segmentation and reduce observer bias. Despite the initial potential of using the tropoelastin

agent for imaging human plaques further optimisation and extensive safety checks will be needed prior to using this agent for *in vivo* imaging of tropoelastin in man.

Conclusions

We demonstrate the development of a new tropoelastin-binding contrast agent and the first *in vivo* implementation of molecular imaging of tropoelastin in animal models of plaque progression and instability, and show uptake of the agent human carotid plaques *ex vivo*. Tropoelastin may represent a new imaging biomarker for plaque progression and instability and for the monitoring of the effectiveness of therapeutic interventions.

Supplementary Material

Refer to Web version on PubMed Central for supplementary material.

Acknowledgments

We acknowledge Drs Maria Thanou and Michael Wright (Institute of Pharmaceutical Science, KCL) for their input on the *in vitro* binding assays. We thank Dr Éva Tóth (Centre de Biophysique Moléculaire, CNRS, Orléans, France) for access to the relaxometer, advice and analysis of those measurements. We also thank David Onthank Lantheus Medical Imaging (North Billerica, USA) who provided the Gd-ESMA for the experiments.

Sources of Funding

This study was funded by the British Heart Foundation (RG/12/1/29262), the BHF Centre of Excellence (RE/08/03) and the Chilean Agency of Technology and Science (CONICYT - PIA - Anillo ACT1416) and by the EU's H2020 research and innovation program under the grant agreement No. 633937 (SPCCT). This work was also supported by the Wellcome EPSRC Centre for Medical Engineering at King's College London (WT 203148/Z/16/Z) and the Department of Health through the National Institute for Health Research (NIHR) comprehensive Biomedical Research Centre award to Guy's & St Thomas' NHS Foundation Trust in partnership with King's College London and King's College Hospital NHS Foundation Trust.

References

1. Sidney S, Rosamond WD, Howard VJ, Luepker RV, National Forum for Heart D and Stroke P. The "heart disease and stroke statistics--2013 update" and the need for a national cardiovascular surveillance system. Circulation. 2013; 127:21–3. [PubMed: 23239838]
2. Cannon B. Cardiovascular disease: Biochemistry to behaviour. Nature. 2013; 493:S2–3. [PubMed: 23364768]
3. Robert L, Robert AM, Jacotot B. Elastin-elastase-atherosclerosis revisited. Arteriosclerosis (Dallas, Tex). 1998; 140:281–95.
4. Maurice P, Blaise S, Gayral S, Debelle L, Laffargue M, Hornebeck W, Duca L. Elastin fragmentation and atherosclerosis progression: the elastokine concept. Trends in cardiovascular medicine. 2013; 23:211–21. [PubMed: 23561795]
5. Brooke BS, Bayes-Genis A, Li DY. New insights into elastin and vascular disease. Trends in cardiovascular medicine. 2003; 13:176–81. [PubMed: 12837579]
6. Krettek A, Sukhova GK, Libby P. Elastogenesis in human arterial disease: a role for macrophages in disordered elastin synthesis. Arteriosclerosis, thrombosis, and vascular biology. 2003; 23:582–7.
7. Haust MD, More RH, Bencosme SA, Balis JU. Elastogenesis in human aorta: an electron microscopic study. Exp Mol Pathol. 1965; 4:508–524. [PubMed: 5847769]
8. Xu C, Zarins CK, Pannaraj PS, Bassiouny HS, Glagov S. Hypercholesterolemia superimposed by experimental hypertension induces differential distribution of collagen and elastin. Arteriosclerosis, thrombosis, and vascular biology. 2000; 20:2566–72.

9. Heinz A, Jung MC, Jahreis G, Rusciani A, Duca L, Debelle L, Weiss AS, Neubert RH, Schmelzer CE. The action of neutrophil serine proteases on elastin and its precursor. Biochimie. 2012; 94:192–202. [PubMed: 22030899]
10. Brooke BS, Bayes-Genis A, Li DY. New Insights into Elastin and Vascular Disease. Trends in cardiovascular medicine. 2003; 13:176–181. [PubMed: 12837579]
11. Wise SG, Weiss AS. Tropoelastin. Int J Biochem Cell Biol. 2009; 41:494–7. [PubMed: 18468477]
12. Hinek A, Rabinovitch M. 67-kD elastin-binding protein is a protective "companion" of extracellular insoluble elastin and intracellular tropoelastin. J Cell Biol. 1994; 126:563–74. [PubMed: 8034752]
13. Moroy G, Ostuni A, Pepe A, Tamburro AM, Alix AJ, Hery-Huynh S. A proposed interaction mechanism between elastin-derived peptides and the elastin/laminin receptor-binding domain. Proteins. 2009; 76:461–76. [PubMed: 19241470]
14. Finnis ML, Gibson MA. Microfibril-associated glycoprotein-1 (MAGP-1) binds to the pepsin-resistant domain of the alpha3(VI) chain of type VI collagen. The Journal of biological chemistry. 1997; 272:22817–23. [PubMed: 9278443]
15. Brown-Augsburger P, Broekelmann T, Mecham L, Mercer R, Gibson MA, Cleary EG, Abrams WR, Rosenbloom J, Mecham RP. Microfibril-associated glycoprotein binds to the carboxyl-terminal domain of tropoelastin and is a substrate for transglutaminase. The Journal of biological chemistry. 1994; 269:28443–9. [PubMed: 7961786]
16. Fischer GM, Swain ML, Cherian K. Increased vascular collagen and elastin synthesis in experimental atherosclerosis in the rabbit. Variation in synthesis among major vessels. Atherosclerosis. 1980; 35:11–20. [PubMed: 7370083]
17. Katsuda S, Kaji T. Atherosclerosis and extracellular matrix. Journal of atherosclerosis and thrombosis. 2003; 10:267–74. [PubMed: 14718743]
18. Gandhi RH, Irizarry E, Cantor JO, Keller S, Nackman GB, Halpern VJ, Newman KM, Tilson MD. Analysis of elastin cross-linking and the connective tissue matrix of abdominal aortic aneurysms. Surgery. 1994; 115:617–20. [PubMed: 8178261]
19. Curran ME, Atkinson DL, Ewart AK, Morris CA, Leppert MF, Keating MT. The elastin gene is disrupted by a translocation associated with supravalvular aortic stenosis. Cell. 1993; 73:159–68. [PubMed: 8096434]
20. Nili N, Zhang M, Strauss BH, Bendeck MP. Biochemical analysis of collagen and elastin synthesis in the balloon injured rat carotid artery. Cardiovascular pathology : the official journal of the Society for Cardiovascular Pathology. 2002; 11:272–6. [PubMed: 12361837]
21. Brasselet C, Durand E, Addad F, Al Haj Zen A, Smeets MB, Laurent-Maquin D, Bouthors S, Bellon G, de Kleijn D, Godeau G, Garnotel R, et al. Collagen and elastin cross-linking: a mechanism of constrictive remodeling after arterial injury. Am J Physiol Heart Circ Physiol. 2005; 289:H2228–33. [PubMed: 15951346]
22. Robinson PN, Arteaga-Solis E, Baldock C, Collod-Beroud G, Booms P, De Paepe A, Dietz HC, Guo G, Handford PA, Judge DP, Kielty CM, et al. The molecular genetics of Marfan syndrome and related disorders. J Med Genet. 2006; 43:769–87. [PubMed: 16571647]
23. Nikkari ST, Jarvelainen HT, Wight TN, Ferguson M, Clowes AW. Smooth muscle cell expression of extracellular matrix genes after arterial injury. The American journal of pathology. 1994; 144:1348–1356. [PubMed: 8203472]
24. Belknap JK, Grieshaber NA, Schwartz PE, Orton EC, Reidy MA, Majack RA. Tropoelastin gene expression in individual vascular smooth muscle cells. Relationship to DNA synthesis during vascular development and after arterial injury. Circulation research. 1996; 78:388–94. [PubMed: 8593697]
25. Rodriguez C, Alcudia JF, Martinez-Gonzalez J, Guadall A, Raposo B, Sanchez-Gomez S, Badimon L. Statins normalize vascular lysyl oxidase down-regulation induced by proatherogenic risk factors. Cardiovascular research. 2009; 83:595–603. [PubMed: 19406911]
26. Rodriguez C, Alcudia JF, Martinez-Gonzalez J, Raposo B, Navarro MA, Badimon L. Lysyl oxidase (LOX) down-regulation by TNFalpha: a new mechanism underlying TNFalpha-induced endothelial dysfunction. Atherosclerosis. 2008; 196:558–64. [PubMed: 17673218]

Europe PMC Funders Author Manuscripts

27. Rodriguez C, Martinez-Gonzalez J, Raposo B, Alcudia JF, Guadall A, Badimon L. Regulation of lysyl oxidase in vascular cells: lysyl oxidase as a new player in cardiovascular diseases. Cardiovascular research. 2008; 79:7–13. [PubMed: 18469024]
28. Rodriguez C, Raposo B, Martinez-Gonzalez J, Casani L, Badimon L. Low density lipoproteins downregulate lysyl oxidase in vascular endothelial cells and the arterial wall. Arteriosclerosis, thrombosis, and vascular biology. 2002; 22:1409–14.
29. Huffman MD, Curci JA, Moore G, Kerns DB, Starcher BC, Thompson RW. Functional importance of connective tissue repair during the development of experimental abdominal aortic aneurysms. Surgery. 2000; 128:429–38. [PubMed: 10965315]
30. Maki JM, Rasanen J, Tikkanen H, Sormunen R, Makikallio K, Kivirikko KI, Soininen R. Inactivation of the lysyl oxidase gene Lox leads to aortic aneurysms, cardiovascular dysfunction, and perinatal death in mice. Circulation. 2002; 106:2503–9. [PubMed: 12417550]
31. Li DY, Brooke B, Davis EC, Mecham RP, Sorensen LK, Boak BB, Eichwald E, Keating MT. Elastin is an essential determinant of arterial morphogenesis. Nature. 1998; 393:276–280. [PubMed: 9607766]
32. Van Herck JL, De Meyer GR, Martinet W, Van Hove CE, Foubert K, Theunis MH, Apers S, Bult H, Vrints CJ, Herman AG. Impaired fibrillin-1 function promotes features of plaque instability in apolipoprotein E-deficient mice. Circulation. 2009; 120:2478–87. [PubMed: 19948973]
33. Van der Donckt C, Van Herck JL, Schrijvers DM, Vanhoutte G, Verhoye M, Blockx I, Van Der Linden A, Bauters D, Lijnen HR, Sluimer JC, Roth L, et al. Elastin fragmentation in atherosclerotic mice leads to intraplaque neovascularization, plaque rupture, myocardial infarction, stroke, and sudden death. European heart journal. 2015; 36:1049–58. [PubMed: 24553721]
34. Senior RM, Griffin GL, Mecham RP. Chemotactic activity of elastin-derived peptides. The Journal of clinical investigation. 1980; 66:859–62. [PubMed: 6903189]
35. Onthank D, Yalamanchili P, Cesati R, Lazewatsky J, Azure M, Hayes M, Kavosi M, Spencer K, Sousa D, Wexler E, Lamoy M, et al. Abstract 1914: BMS753951: A Novel Low Molecular Weight Magnetic Resonance Contrast Agent Selective For Arterial Wall Imaging. Circulation. 2007; 116(II):411–412. [PubMed: 17606844]
36. Makowski MR, Wiethoff AJ, Blume U, Cuello F, Warley A, Jansen CH, Nagel E, Razavi R, Onthank DC, Cesati RR, Marber MS, et al. Assessment of atherosclerotic plaque burden with an elastin-specific magnetic resonance contrast agent. Nature medicine. 2011; 17:383–8.
37. Phinikaridou A, Andia ME, Indermuehle A, Onthank DC, Cesati RR, Smith A, Robinson SP, Saha P, Botnar RM. Vascular remodeling and plaque vulnerability in a rabbit model of atherosclerosis: comparison of delayed-enhancement MR imaging with an elastin-specific contrast agent and unenhanced black-blood MR imaging. Radiology. 2014; 271:390–9. [PubMed: 24475852]
38. Makowski MR, Preissel A, von Bary C, Warley A, Schachoff S, Keithan A, Cesati RR, Onthank DC, Schwaiger M, Robinson SP, Botnar RM. Three-dimensional imaging of the aortic vessel wall using an elastin-specific magnetic resonance contrast agent. Investigative radiology. 2012; 47:438–44. [PubMed: 22627945]
39. Botnar RM, Wiethoff AJ, Ebersberger U, Lacerda S, Blume U, Warley A, Jansen CH, Onthank DC, Cesati RR, Razavi R, Marber MS, et al. In vivo assessment of aortic aneurysm wall integrity using elastin-specific molecular magnetic resonance imaging. Circulation Cardiovascular imaging. 2014; 7:679–89. [PubMed: 24871347]
40. von Bary C, Makowski M, Preissel A, Keithahn A, Warley A, Spuentrup E, Buecker A, Lazewatsky J, Cesati R, Onthank D, Schickl N, et al. MRI of coronary wall remodeling in a swine model of coronary injury using an elastin-binding contrast agent. Circulation Cardiovascular imaging. 2011; 4:147–55. [PubMed: 21378029]
41. Wildgruber M, Bielicki I, Aichler M, Kosanke K, Feuchtinger A, Settles M, Onthank DC, Cesati RR, Robinson SP, Huber AM, Rummeny EJ, et al. Assessment of myocardial infarction and postinfarction scar remodeling with an elastin-specific magnetic resonance agent. Circulation Cardiovascular imaging. 2014; 7:321–9. [PubMed: 24363356]
42. Protti A, Lavin B, Dong X, Lorrio S, Robinson S, Onthank D, Shah AM, Botnar RM. Assessment of Myocardial Remodeling Using an Elastin/Tropoelastin Specific Agent with High Field Magnetic Resonance Imaging (MRI). Journal of the American Heart Association. 2015; 4:e001851. [PubMed: 26272655]

43. Chen W, Cormode DP, Vengrenyuk Y, Herranz B, Feig JE, Klink A, Mulder WJ, Fisher EA, Fayad ZA. Collagen-specific peptide conjugated HDL nanoparticles as MRI contrast agent to evaluate compositional changes in atherosclerotic plaque regression. JACC Cardiovasc Imaging. 2013; 6:373–84. [PubMed: 23433925]
44. Christov A, Korol RM, Dai E, Liu L, Guan H, Bernards MA, Cavers PB, Susko D, Lucas A. In vivo optical analysis of quantitative changes in collagen and elastin during arterial remodeling. Photochemistry and photobiology. 2005; 81:457–66. [PubMed: 15560737]
45. Phinikaridou A, Hallock KJ, Qiao Y, Hamilton JA. A robust rabbit model of human atherosclerosis and atherothrombosis. J Lipid Res. 2009; 50:787–97. [PubMed: 19141434]
46. Phinikaridou A, Ruberg FL, Hallock KJ, Qiao Y, Hua N, Viereck J, Hamilton JA. In vivo detection of vulnerable atherosclerotic plaque by MRI in a rabbit model. Circulation Cardiovascular imaging. 2010; 3:323–32. [PubMed: 20194634]
47. Caravan P, Ellison JJ, McMurry TJ, Lauffer RB. Gadolinium(III) Chelates as MRI Contrast Agents: Structure, Dynamics, and Applications. Chem Rev. 1999; 99:2293–352. [PubMed: 11749483]
48. Phinikaridou A, Hua N, Pham T, Hamilton JA. Regions of low endothelial shear stress colocalize with positive vascular remodeling and atherosclerotic plaque disruption: an in vivo magnetic resonance imaging study. Circulation Cardiovascular imaging. 2013; 6:302–10. [PubMed: 23357244]
49. Overoye-Chan K, Koerner S, Looby RJ, Kolodziej AF, Zech SG, Deng Q, Chasse JM, McMurry TJ, Caravan P. EP-2104R: a fibrin-specific gadolinium-Based MRI contrast agent for detection of thrombus. Journal of the American Chemical Society. 2008; 130:6025–39. [PubMed: 18393503]
50. Caravan P, Das B, Dumas S, Epstein FH, Helm PA, Jacques V, Koerner S, Kolodziej A, Shen L, Sun WC, Zhang Z. Collagen-targeted MRI contrast agent for molecular imaging of fibrosis. Angewandte Chemie. 2007; 46:8171–3. [PubMed: 17893943]
51. Spuentrup E, Ruhl KM, Botnar RM, Wiethoff AJ, Buhl A, Jacques V, Greenfield MT, Krombach GA, Gunther RW, Vangel MG, Caravan P. Molecular magnetic resonance imaging of myocardial perfusion with EP-3600, a collagen-specific contrast agent: initial feasibility study in a swine model. Circulation. 2009; 119:1768–75. [PubMed: 19307474]
52. Hinek A, Rabinovitch M, Keeley F, Okamura-Oho Y, Callahan J. The 67-kD elastin/laminin-binding protein is related to an enzymatically inactive, alternatively spliced form of beta-galactosidase. The Journal of clinical investigation. 1993; 91:1198–205. [PubMed: 8383699]
53. Houghton AM, Quintero PA, Perkins DL, Kobayashi DK, Kelley DG, Marconcini LA, Mecham RP, Senior RM, Shapiro SD. Elastin fragments drive disease progression in a murine model of emphysema. The Journal of clinical investigation. 2006; 116:753–9. [PubMed: 16470245]
54. Badesch DB, Lee PD, Parks WC, Stenmark KR. Insulin-like growth factor I stimulates elastin synthesis by bovine pulmonary arterial smooth muscle cells. Biochemical and biophysical research communications. 1989; 160:382–7. [PubMed: 2653320]

Europe PMC Funders Author Manuscripts

Europe PMC Funders Author Manuscripts

Clinical Perspectives

A tropoelastin-binding peptide labeled with gadolinium is a novel probe for molecular imaging of dysfunctional elastogenesis by *in vivo* MRI. Our new probe combined with quantitative T_1 mapping may be used as a new imaging biomarker to quantify ineffective elastogenesis related to plaque progression and instability and identify plaques that may be susceptible to rupture.

Molecular imaging of tropoelastin using our presented imaging approach may provide information on plaque progression and instability and for monitoring the effectiveness of established and novel interventions in different animal models and human tissue. We showed that statins, a widely used intervention, reduced tropoelastin accumulation in atherosclerotic plaques but the long term effects on plaque stability remains to be elucidated. Similarly, the effectiveness of novel interventions, that specifically aim elastin remodeling, can be and remain to be investigated using this contrast agent. Importantly, in our work we implemented MRI protocols that have already been used in the clinical setting enabling translation of our current findings in bigger animal models of coronary atherosclerosis to identify plaques that may be susceptible to rupture.

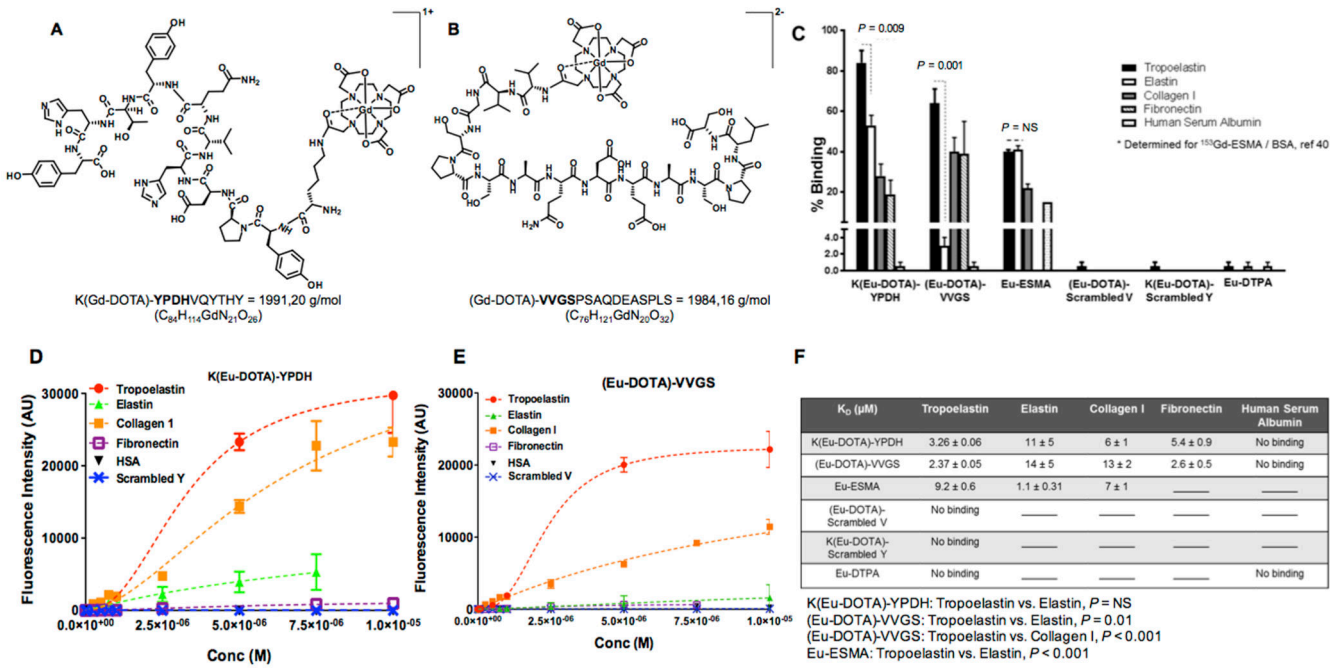

K_D (μM)	Tropoelastin	Elastin	Collagen I	Fibronectin	Human Serum Albumin
K(Eu-DOTA)-YPDH	3.26 ± 0.06	11 ± 5	6 ± 1	5.4 ± 0.9	No binding
(Eu-DOTA)-VVGS	2.37 ± 0.05	14 ± 5	13 ± 2	2.6 ± 0.5	No binding
Eu-ESMA	9.2 ± 0.6	1.1 ± 0.31	7 ± 1	____	____
(Eu-DOTA)-Scrambled V	No binding	____	____	____	____
K(Eu-DOTA)-Scrambled Y	No binding	____	____	____	____
Eu-DTPA	No binding	____	____	____	No binding

Figure 1. Chemical structures and *in vitro* binding experiments of the tropoelastin-binding probes.

A, B, Chemical structures of the probes. **C,** *In vitro* binding show superior discrimination between tropoelastin and mature elastin for the (Eu-DOTA)-VVGS compared with K(Eu-DOTA)-YPDH whereas Eu-ESMA binds equally to tropoelastin and mature elastin. The new probes show less binding towards other proteins compared with tropoelastin whereas the scrambled peptides do not bind to tropoelastin. Eu-DTPA shows little binding to tropoelastin, collagen I and human serum albumin. **D-E,** The saturation binding plots show that both probes bind to tropoelastin whereas no binding to HSA was observed. Finally, no binding of the scrambled probes to tropoelastin was observed. **F,** The K_D values showed that the probes have high affinity for tropoelastin. Statistical differences between Kd values are shown.

No binding signifies that the data could not be fit, and lines indicate that the assay was not performed (n=2 for elastin, n=3 for all other proteins). Eu: europium(III), ESMA: elastin-specific MR contrast agent.

Europe PMC Funders Author Manuscripts

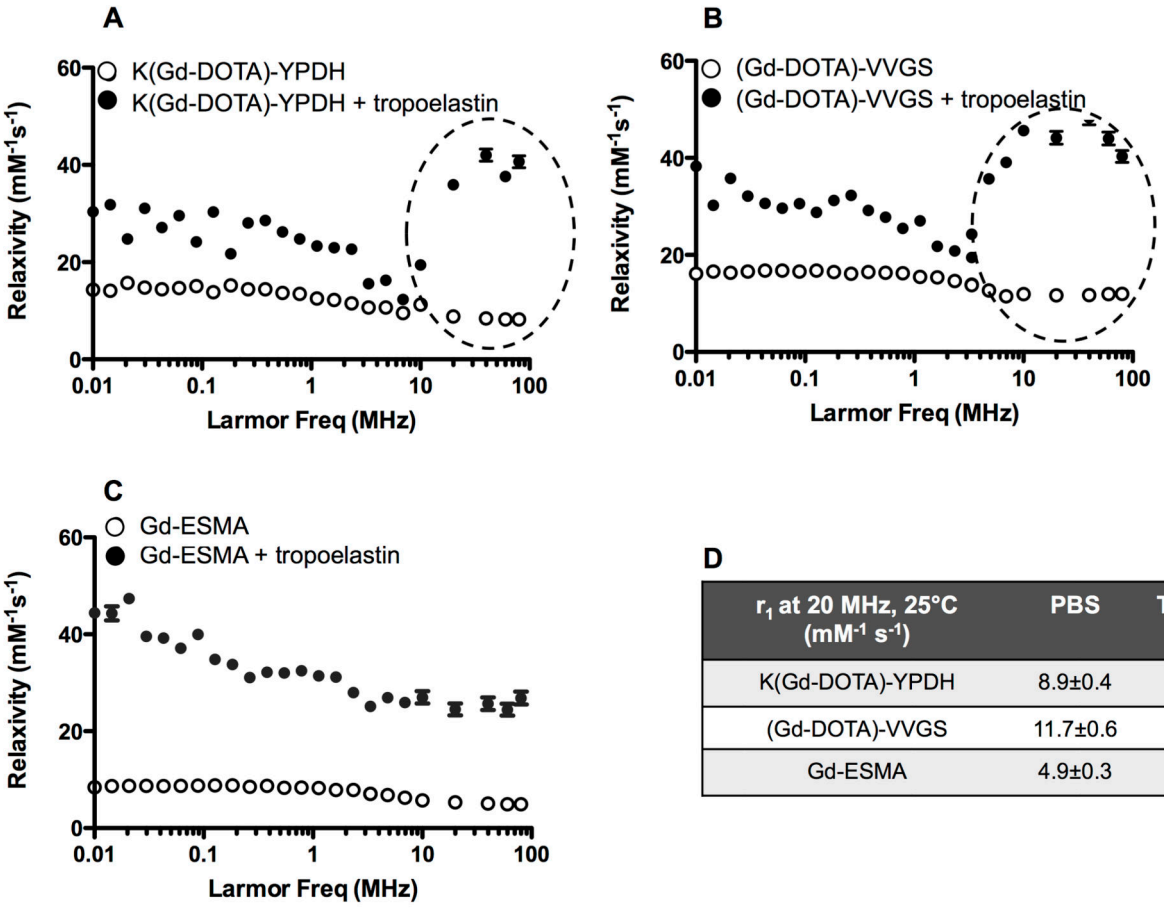

D

r_1 at 20 MHz, 25°C (mM^{-1} s^{-1})	PBS	Tropoelastin
K(Gd-DOTA)-YPDH	8.9±0.4	36±1
(Gd-DOTA)-VVGS	11.7±0.6	44±1
Gd-ESMA	4.9±0.3	25±1

Figure 2. Relaxivity studies and nuclear magnetic relaxation dispersion (NMRD) profiles of Gd-labeled tropoelastin and elastin-binding contrast agents at 20MHz and 37°C.

A-C, ^{1}H-NMRD in the absence (open circles) and presence (black circles) of tropoelastin. The profiles obtained in PBS (open circles) are characteristic of small-molecular weight complexes. In the presence of tropoelastin (black circles), the relaxivity increases suggesting binding of the probes to the protein. The relaxivity increase was more evident for both (Gd-DOTA)-VVGS and K(Gd-DOTA)-YPDH, compared with Gd-ESMA. **D,** Summary of the relaxivity values, (n=3 for all studies).

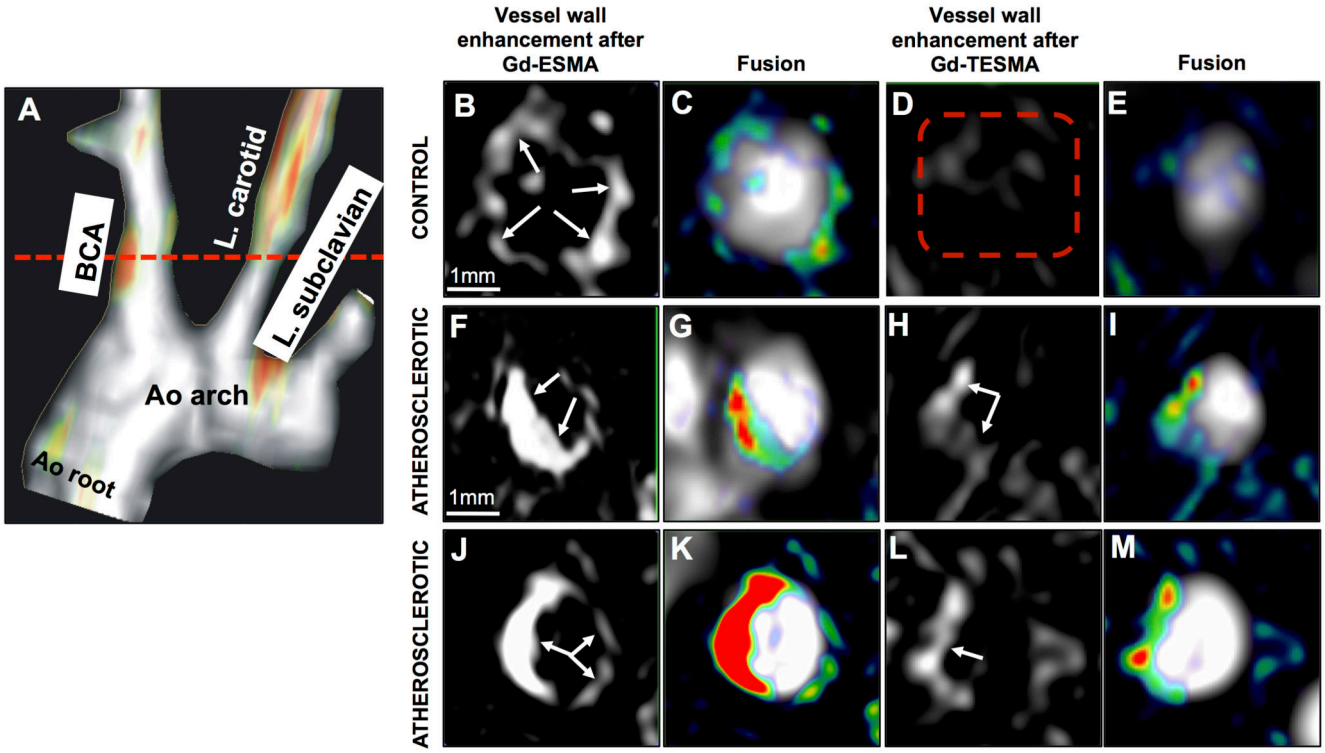

Figure 3. ***In vivo*** **MRI comparison of vessel wall enhancement using the elastin (ESMA) and tropoelastin (TESMA) binding contrast agents in mice.**

A, Fused MIP reconstructed MRA and DE-MRI images after administration of Gd-TESMA show focal uptake of Gd-TESMA in the BCA of an atherosclerotic ApoE$^{-/-}$ mouse. **B-E,** MRI images of the BCA acquired from a control animal, scanned 24h apart, showed vessel wall uptake of Gd-ESMA **(B, C)** but no uptake of Gd-TESMA **(D, E)** due to the lack of tropoelastin in the absence of disease. **F-M,** MRI images of the BCA acquired from two different diseased animals showed enhancement of the vessel wall after administration of both agents due to the presence of both cross-linked elastin and tropoelastin in the atherosclerotic lesion. MIP: maximum intensity projection, BCA: brachiocephalic artery. L.: left, Ao: aortic, (n=5 per group).

Europe PMC Funders Author Manuscripts

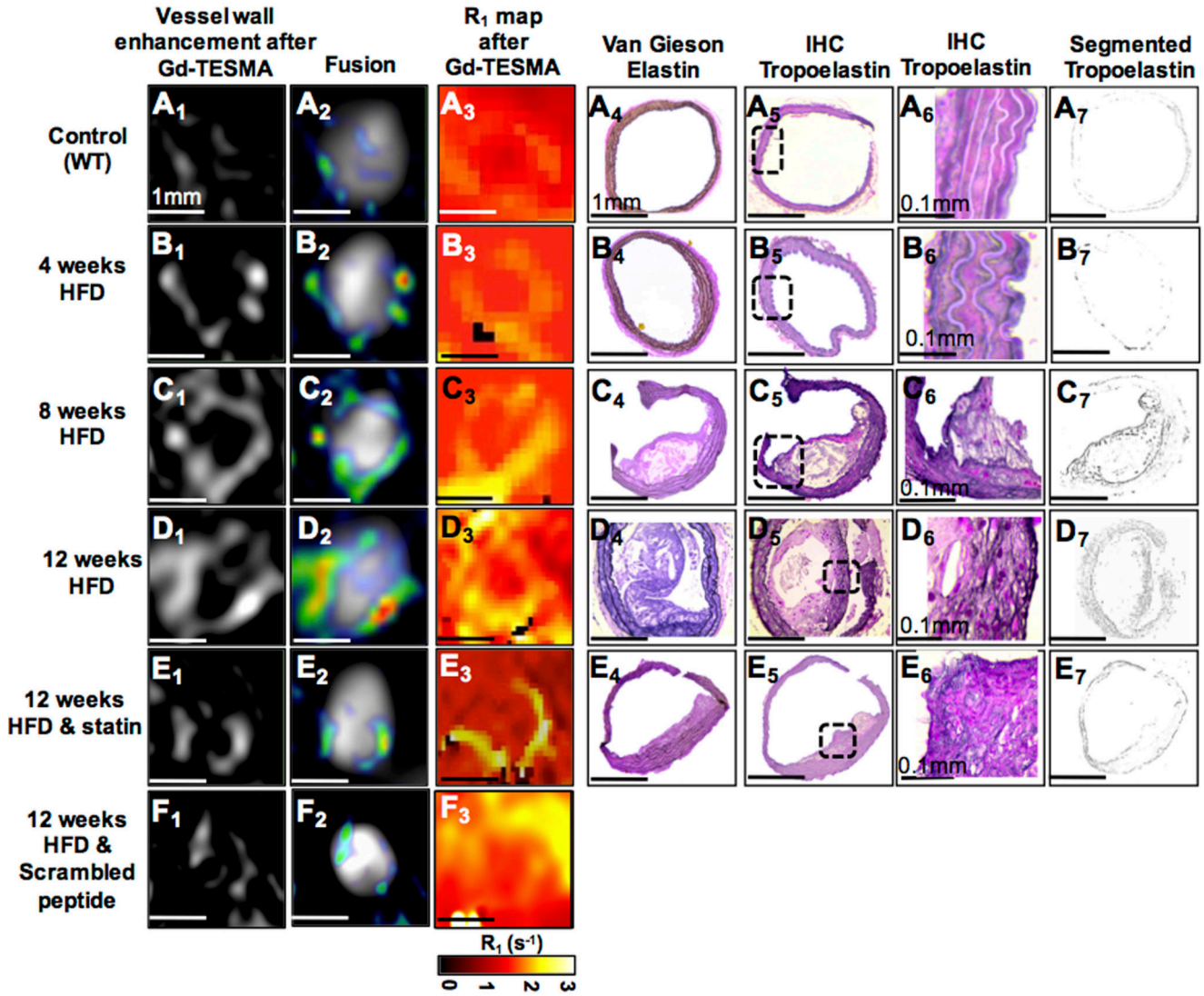

Figure 4. Molecular *in vivo* MRI of tropoelastin in atherosclerotic mice.

A_1-E_1 & A_2-E_2 & A_3-E_3, DE-MRI images and R_1 relaxation rate maps after injection of Gd-TESMA show progressive enhancement of the brachiocephalic artery and vessel wall relaxation rate with disease progression compared with control and statin-treated mice. **F_1-F_3,** DE-MRI and R_1 maps after injecting the scrambled peptide (DOTA-GAESAPLVSSVQSPD) shows less vessel wall enhancement and relaxation rate. **A_4-E_4,** Van Gieson elastin staining shows the development of atherosclerotic lesions. **A_5-E_5, A_6-E_6 and A_7-E_7,** Immunohistochemistry shows accumulation of tropoelastin molecules (dark purple staining) in the lesion (n=10 per group). DE-MRI: delayed-enhanced MRI, TESMA: tropoelastin-specific MR contrast agent, HFD: high-fat diet.

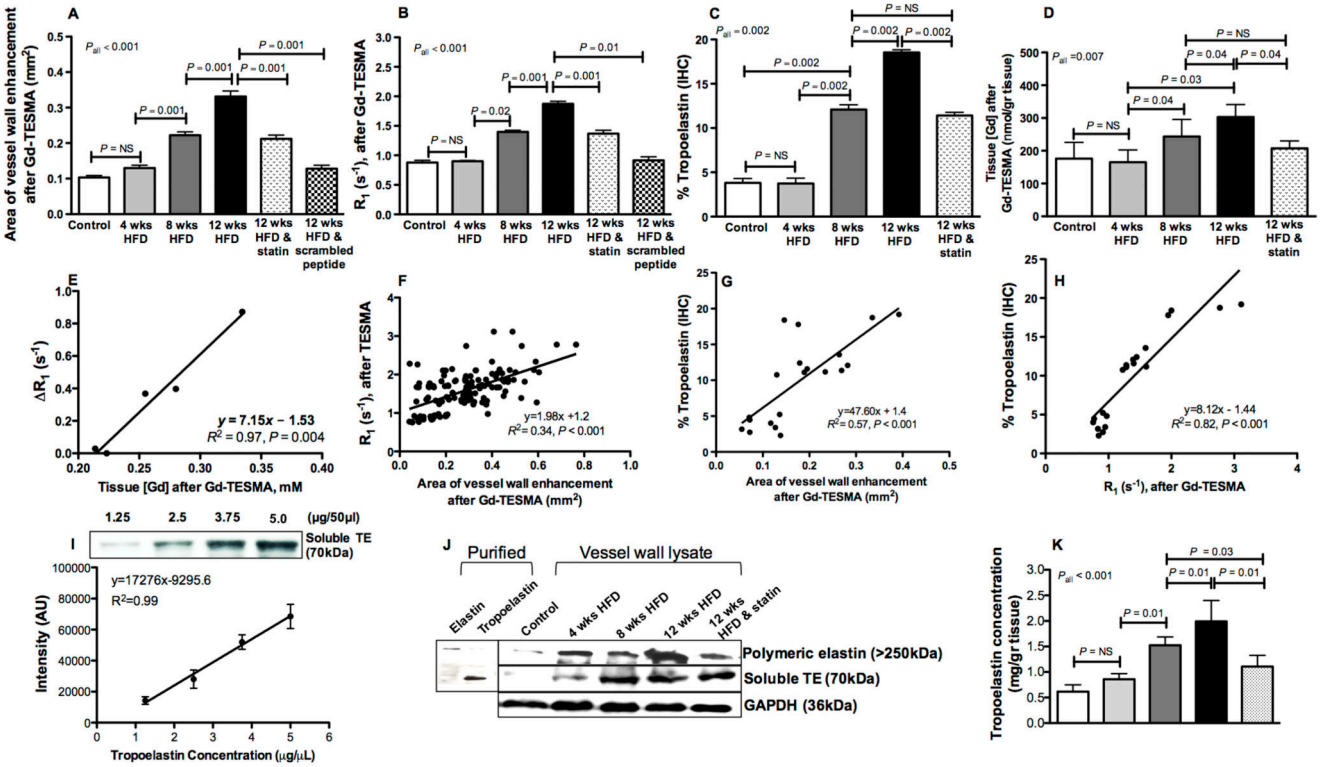

Figure 5. Quantitative MRI, histology and western blotting of murine vessel wall tropoelastin.

A-B, DE-MRI area and vessel wall R_1 measured after administration of Gd-TESMA increase with disease progression and decrease with statin-treatment (n=10 per group). **C,** Tropoelastin accumulates during atherosclerosis progression and reduces in statin-treated mice (n=4 per group). **D,** Vessel wall gadolinium concentration increases with disease progression (n=4 per group). **E,** The measured *in vivo* bound relaxivity of TESMA is r_1=7.15 $mM^{-1}s^{-1}$. **F,** DE-MRI area correlates with vessel wall R_1 measured after administration of Gd-TESMA (n=10 per group). **G-H,** The tropoelastin content measured histologically correlates with both the DE-MRI (G) and vessel wall R_1 relaxation rate (H) measured by MRI after administration of Gd-TESMA (n=4 per group). **I,** Dilutions of recombinant human tropoelastin were used to generate a standard curve for the quantification of the tropoelastin concentration from tissue lysates using western blotting. **J,** Western blotting of purified elastin showed that cross-linked elastin is an insoluble polymer with a high molecular band (>250kDa) whereas soluble tropoelastin has a molecular weight at 70kDa. Western blotting for tropoelastin extracted from the vessel wall (n=3 per group) showed negligible amounts in control arteries and increased deposition of the protein during atherosclerosis progression in $ApoE^{-/-}$ mice. Tropoelastin content was decreased in the statin-treated $ApoE^{-/-}$ mice. **K,** Quantification of tropoelastin concentration in control and diseased arteries as measured by western blotting.

Europe PMC Funders Author Manuscripts

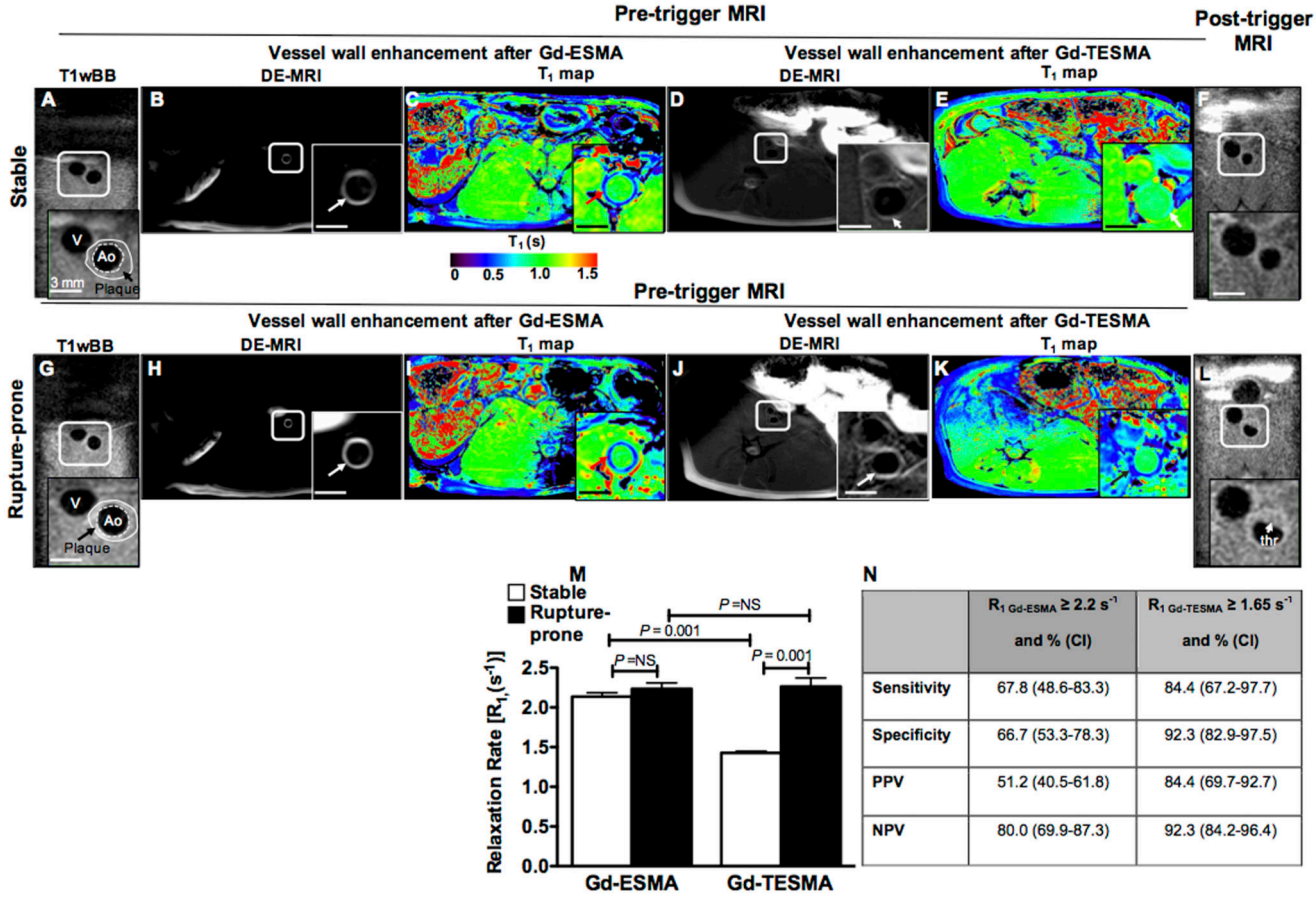

Figure 6. ***In vivo*** **molecular MRI of tropoelastin allows detection of rupture-prone rabbit plaque.** Pre-trigger and post-trigger MRI images of rabbit stable (A-F) and rupture-prone (G-L) plaques. **A,G,** Pre-trigger native zoom T1wBB images show the plaque. **B, H, C, I,** Delayed-enhanced inversion recovery images and T_1 maps after administration of Gd-ESMA show a strong enhancement of the aortic wall and shortening of the T_1 relaxation time in both stable and rupture-prone plaque. **D, J, E, K,** Corresponding delayed-enhanced inversion recovery images after administration of Gd-TESMA show vessel wall enhancement and lower T1 values in ruptured-prone compared with stable plaque. **F, L,** Corresponding native zoom T1wBB post-trigger images show the presence of thrombus only at the side of the ruptured plaque. **M,** Quantification of vessel wall R_1 relaxation rate show a significantly higher R_1 value in rupture-prone compared with stable plaque only after administration of Gd-TESMA.

Europe PMC Funders Author Manuscripts

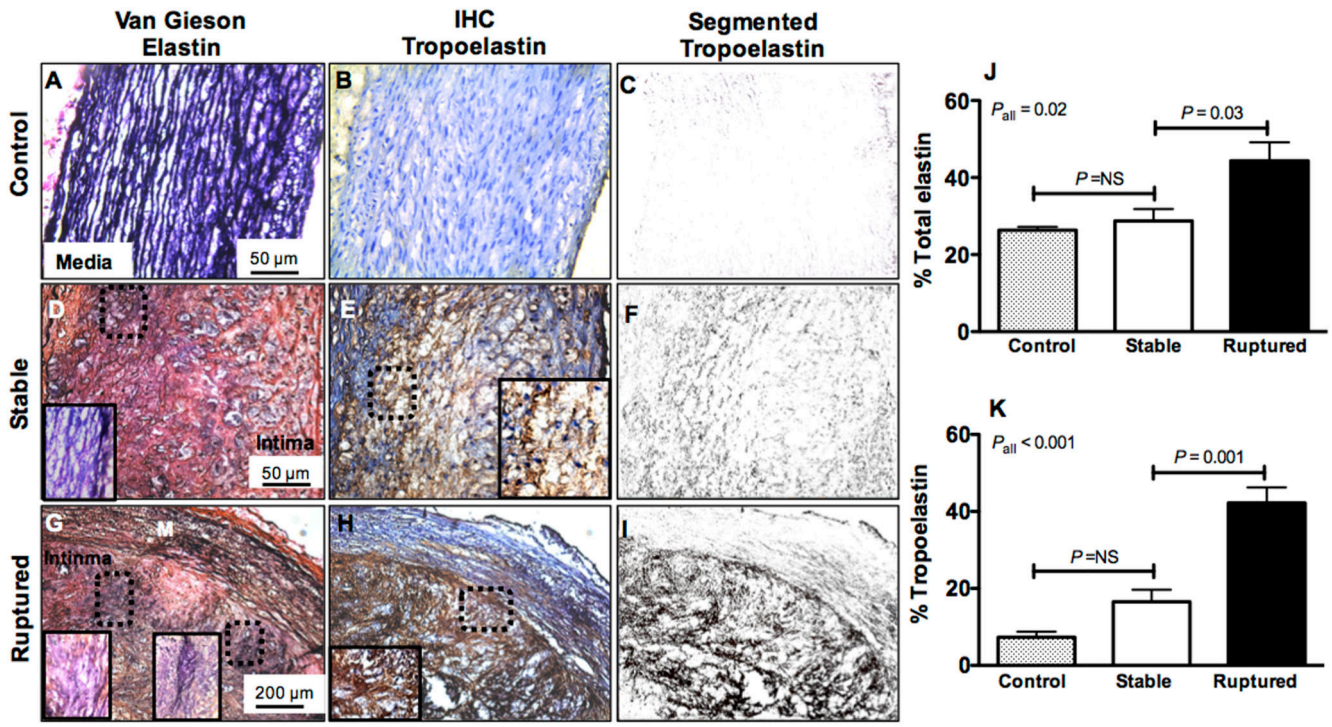

Figure 7. Histological analyses show accumulation of tropoelastin in rabbit rupture-prone compared with stable plaque.

A, D, G, Van Gieson elastin staining (dark purple indicates elastin fibers) shows the presence of organized elastin fibers in the media of control tissue and a net accumulation of elastin fibers in the intima of stable and rupture-prone plaque. **B-C, E-F, H-I,** Corresponding immunohistochemistry for tropoelastin (brown staining) shows lack of tropoelastin positive fibers in control aortas, upregulation in stable and deposition of a dense network of tropoelastin fibers in rupture-prone plaque. **J-K,** Quantification of total elastin and tropoelastin shows significantly higher tropoelastin in ruptured compared with stable plaque.

Europe PMC Funders Author Manuscripts

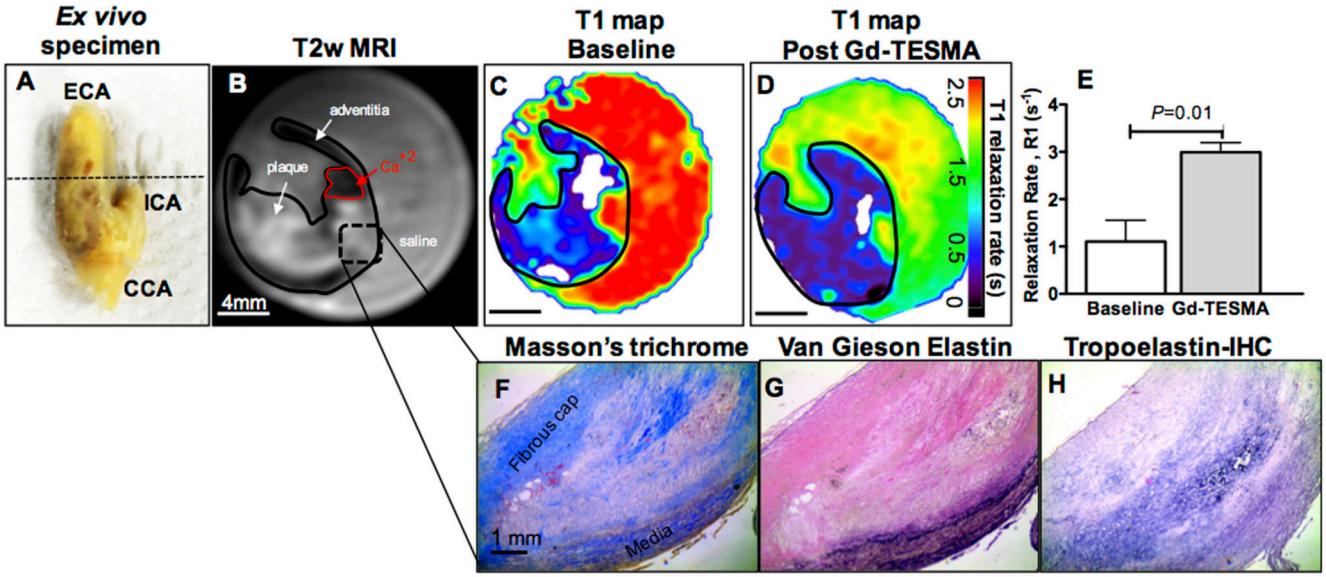

Figure 8. ***Ex vivo*** **T1 mapping experiments using human carotid endarterectomy specimens at 3T.**

A, *Ex vivo* photograph of an excised left carotid artery. **B-C,** A T2w image shows the plaque in the internal carotid artery (B) and a corresponding T1 map shows the baseline relaxation values (C). **D,** A repeated T1 mapping experiment after soaking the specimen in Gd-TESMA shows a reduction of the T1 values. **E,** Quantification of the changes shows a significant uptake of Gd-TESMA in human carotid plaques. **F-G,** Corresponding histology shows the lesion (F-G) and the deposition of tropoelastin (dark purple staining) (H).

Europe PMC Funders Author Manuscripts